



ELSEVIER

Physica D 97 (1996) 253–263

PHYSICA D

Influence of boundaries on pattern selection in through-flow [★]

D. Roth ^a, P. Büchel ^a, M. Lücke ^{a,*}, H.W. Müller ^a, M. Kamps ^b, R. Schmitz ^c^a *Institut für Theoretische Physik, Universität des Saarlandes, D-66041 Saarbrücken, Germany*^b *Höchstleistungsrechenzentrum, Forschungszentrum, D-52425 Jülich, Germany*^c *Institut für Festkörperforschung, Forschungszentrum, D-52425 Jülich, Germany*

Abstract

The problem of pattern selection in *absolutely* unstable open flow systems is investigated by considering the example of Rayleigh–Bénard convection. The spatio-temporal structure of convection rolls propagating downstream in an externally imposed flow is determined for six different inlet/outlet boundary conditions. Results are obtained by numerical simulations of the Navier–Stokes equations and by comparison with the corresponding Ginzburg–Landau amplitude equation. A unique selection process is observed being a function of the control parameters and the boundary conditions but independent of history and system length. The problem can be formulated in terms of a nonlinear eigen/boundary value problem where the frequency of the propagating pattern is the eigenvalue.

PACS: 47.54.+r; 47.20.Bp; 47.27.Te; 47.20.Ky

1. Introduction

The spontaneous formation of patterns in dissipative systems with a continuous energy supply is a commonly observed phenomenon [1]. Classical examples are the generation of rolls in Rayleigh–Bénard convection (RBC) [1,2] and Taylor vortex flow (TVF) in the annulus between two concentric cylinders [1,3]. If the forcing is sufficiently strong, patterns bifurcate out of a homogeneous basic state and often show a periodic structure in space and/or in time. For a given set of parameters and boundary conditions (BCs) one frequently observes a discrete or continuous spectrum of allowed wave numbers and frequencies. The initial conditions finally determine which ones are selected.

Usually secondary instabilities limit the range of stable existence in parameter space. Recent numerical simulations of RBC [4–6] and TVF [7] suggest that this degeneracy of stable stationary patterns is lifted as soon as a flow through the system is imposed. These “open flow systems” exhibit a pattern selection mechanism which *uniquely* fixes the dissipative structure.

Spatially localized perturbations in open flow systems are advected by the flow. Depending on whether the trailing front of a growing perturbation of the basic state propagates within a linear analysis in the downstream or in the upstream direction the system is convectively or absolutely unstable, respectively [8]. The property of absolute or convective instability can be controlled externally by tuning the strength of the imposed flow [9–12]. However, this distinction was made only in the more recent experiments [11,12]. Pattern formation in convectively unstable systems requires a

[★] Dedicated to Prof. F. H. Busse on the occasion of his 60th birthday.

* Corresponding author. E-mail: luecke@lusi.uni-sb.de.

permanent source of disturbances in order to sustain steady convection [13]. The spatiotemporal behavior of such “noise sustained structures” sensitively depends on the details of the perturbation source [11,12].

The present paper, however, deals with the absolutely unstable situation where the nonlinear structures are self-sustained and stable. They are characterized in the longtime limit by time periodic fields with characteristic streamwise field profiles and wave number profiles. The frequency associated with the downstream motion of the pattern turns out to be constant in space and time. For a given set of control parameters and BCs the pattern in the absolutely unstable regime is independent of initial conditions and history.

In this paper we deal with RBC subject to an imposed lateral shear flow, i.e., with convection rolls propagating in downstream direction. A related investigation of TVF has been published elsewhere [7]. Different kinds of inlet and outlet BCs are considered and their influence upon the convection structures is systematically investigated. To this end we perform computer simulations of the full hydrodynamical field equations that we refer to as Navier–Stokes equations (NSE). The results are compared with analytical and numerical solutions of the corresponding Ginzburg–Landau equation (GLE). The amplitude equation most clearly reveals that the selection process can be understood as a nonlinear eigenvalue problem [7]: The frequency plays the role of the eigenvalue, while the set of hydrodynamic fields is the associated eigenfunction. Then the selection seems to result from requiring the spatial variation of pattern envelope and phase to be as small as possible under the imposed inlet/outlet BC which is analogous to ground state properties of the linear stationary Schrödinger equation.

The paper is organized as follows: Section 2 specifies the system, the BCs for the simulations, and the methods of investigation. Section 3 recapitulates pattern selection properties in the presence of through-flow within the GLE. This provides a useful frame work for the interpretation of our results. The latter ones are presented in Section 4 which forms the main part of our paper. A comprehensive analysis of the convection patterns is given and a discussion of the influence of BCs on spatiotemporal properties

of the selected structures as a function of through-flow rate. The conclusion gives a short summary of our results.

2. The system

We investigate properties of convection rolls in a viscous, incompressible fluid layer, that is heated from below in a homogeneous gravitational field directed downwards. In addition we impose a lateral through-flow.

2.1. Equations

The system is described by the balance equations for mass, heat, and momentum in Oberbeck–Boussinesq approximation [10,14–16]:

$$0 = -\nabla \cdot \mathbf{u}, \quad (2.1)$$

$$\partial_t T = -\nabla \cdot \mathbf{Q}; \quad \mathbf{Q} = \mathbf{u}T - \nabla T, \quad (2.2)$$

$$\partial_t \mathbf{u} = -\nabla (\mathbf{u} : \mathbf{u} + p - \sigma \nabla : \mathbf{u}) + \sigma R T \mathbf{e}_z, \quad (2.3)$$

which we shall refer to as Navier–Stokes equations (NSE). Lengths are scaled by the thickness of the layer d , times by the vertical thermal diffusion time d^2/κ , and the velocity field $\mathbf{u} = (u, v, w)$ by κ/d . Here T denotes the deviation of the temperature from the mean temperature T_0 in the fluid measured in units of the temperature difference ΔT between the plates and p is the reduced pressure. The ratio of the momentum diffusivity ν and thermal diffusivity κ , i.e., the Prandtl number $\sigma = \nu/\kappa$, is the material parameter characterizing the fluid. The through-flow is in positive x -direction, with the inlet at $x = 0$ and the outlet at $x = L$. In the vertical direction the lower plate is located at $z = 0$, whereas the upper one is at $z = 1$.

The system is characterized by two control parameters: The Rayleigh number

$$Ra = \frac{\alpha g d^3 \Delta T}{\kappa \nu} \quad (2.4)$$

measures the heating and the Reynolds number

$$Re = \frac{\bar{U} d}{\nu} \quad (2.5)$$

measures the through-flow rate. Here α denotes the thermal expansion coefficient of the fluid, g is the gravitational acceleration, and \bar{U} the vertical average of the imposed lateral through-flow.

2.2. Conductive state

For small Rayleigh numbers one observes a homogeneous basic state with a linear conductive temperature profile T_{cond} and a parabolic Poiseuille profile $U(z)$ of the velocity field

$$\mathbf{u}_{\text{cond}} = U(z)\mathbf{e}_x; \quad U(z) = 6\sigma Re z(1 - z); \quad (2.6)$$

$$T_{\text{cond}} = \frac{1}{2} - z, \quad (2.7)$$

which is globally stable for small thermal stress. Note that the effective through-flow strength is given by the Peclet number $Pe = \sigma Re$. We have investigated in this work the case $\sigma = 1$. Thus, the comparison of through-flow induced effects in fluids of other σ has to be based on common Peclet numbers.

2.3. Transverse convection rolls

At a critical Rayleigh number $Ra_c(Re)$ [4,5,17] a laterally periodic solution describing downstream traveling transverse convection rolls with axes perpendicular to the through-flow direction bifurcates out of the basic state. For convenience we introduce the relative deviation

$$\mu = Ra/Ra_c(Re) - 1 \quad (2.8)$$

from the threshold as a new parameter measuring the externally imposed thermal stress. We also use the reduced distance

$$\epsilon = Ra/Ra_c^0 - 1 \quad (2.9)$$

from the threshold Ra_c^0 for zero through-flow such that

$$\mu = \frac{\epsilon}{1 + \epsilon_c(Re)} \quad (2.10)$$

with $\epsilon_c = Ra_c(Re)/Ra_c^0 - 1$.

In this work we will focus on patterns in which the roll axes are perpendicular to the through-flow direction. They occur as the first instability in narrow

Table 1
Lateral boundary conditions at $x = 0$ and/or $x = L$

Field	Type	Symbol
$w(x, z; t) = 0$	No slip	N
$\partial_x w(x, z; t) = 0$	Free slip	F
$T(x, z; t) = T_{\text{cond}}(z)$	Conductive profile	T_{cond}
$T(x, z; t) = 0$	Mean temperature	T_0
$\partial_x T(x, z; t) = 0$	Insulating	Q_0

convection channels which suppress longitudinal rolls [10,18–21] whereas in laterally unbounded systems the bifurcation threshold for longitudinal rolls is lowest [17]. In our numerical simulations we investigate the x - z plane perpendicular to the roll axes ignoring any spatial variation along the roll axes. Thus we solve the hydrodynamical field equations (2.1)–(2.3) for the lateral velocity component $u(x, z; t)$, the vertical velocity component $w(x, z; t)$, the pressure $p(x, z; t)$, and the temperature field $T(x, z; t)$.

2.4. Boundary conditions

The horizontal BCs are *always* no slip and perfectly heat conducting

$$u = w = 0 \quad \text{at } z = 0, 1, \quad (2.11)$$

$$T = \frac{1}{2} \quad \text{at } z = 0, \quad T = -\frac{1}{2} \quad \text{at } z = 1. \quad (2.12)$$

At the lateral boundaries we *always* enforce the Poiseuille flow profile

$$u(x, z; t) = U(z) \quad \text{at } x = 0, L. \quad (2.13)$$

For the vertical velocity we have applied laterally no slip (N) conditions (cf. Table 1) or free slip (F) conditions. For the temperature field we have investigated the three lateral conditions that are listed in Table 1 and that are abbreviated by the symbols T_{cond} , T_0 , and Q_0 , respectively. We have called the latter thermally insulating since the diffusive part of the heat current Q (2.2) vanishes there. But it should be noted that the lateral Poiseuille flow transports heat advectively through the lateral boundaries. To specify the six possible combinations of $\{N, F\}$ conditions with $\{T_{\text{cond}}, T_0, Q_0\}$ conditions, that we have investigated, we use a two-letter coding. Thus, e.g., N - Q_0 implies $w = 0$ and $\partial_x T = 0$. All numerical solutions have been obtained for a channel length of $L = 50$.

2.5. Methods of investigation

To solve the time dependent 2D NSE (2.1)–(2.3) we used an explicit finite difference numerical code that allows a flexible and convenient incorporation of various BCs and that has been used successfully in related problems [4,5,7]. The final-state solutions obtained in this way represent transverse convection rolls that propagate downstream under a stationary x -dependent intensity envelope. These patterns oscillate in time with a global, i.e., spatially independent frequency ω while wave number k , phase velocity $v_{\text{ph}} = \omega/k$, and convection intensity vary in x -direction. The frequency and the spatial variation of the final pattern depend on Ra , Re , and the BCs but not on parameter history.

To characterize the convection structures we use the convective deviation,

$$\delta u(x, z; t) = u(x, z; t) - U(z), \quad (2.14)$$

of the lateral velocity field from the Poiseuille flow as the order parameter field. Compared with the vertical velocity w or the convective temperature profile $T - T_{\text{cond}}$ this field has some technical advantages (cf. Section 4). After having determined the global oscillation frequency ω of the pattern we perform a temporal Fourier analysis

$$\delta u(x, z; t) = \sum_n \delta u_n(x, z) e^{-in\omega t}. \quad (2.15)$$

The zeroth component $\delta u_0(x, z)$ describes a stationary modification of the basic state's Poiseuille through-flow profile that reflects the presence of a stationary secondary roll vortex system (cf. Section 4). The higher harmonics u_n with $n \geq 2$ are in general small compared to the fundamental mode

$$u_1(x, z) = |u_1(x, z)| e^{i\varphi_1(x, z)}. \quad (2.16)$$

We use $|u_1|$ to characterize the intensity profile of the pattern and we characterize its wave number by $k = \partial_x \varphi_1$. Within the GLE approximation (Section 3) the fields oscillate harmonically in time and only $|u_1|$ is nonzero. Thus the GLE cannot reproduce the stationary secondary vortex flow discussed in Section 4.

3. Pattern selection within the GLE

The selection process for convection patterns in the presence of a lateral flow is a nonlinear eigenvalue/boundary value problem. This is easiest to understand within the GLE approximation [7]. However, one should keep in mind that GLE and NSE results differ systematically.

3.1. GLE for propagating patterns

Within the amplitude equation approximation the convection fields of the propagating pattern of transverse rolls have the form of harmonic waves, e.g.,

$$\delta u(x, z; t) = A(x, t) e^{i(k_c x - \omega_c t)} \hat{u}(z) + \text{c.c.} \quad (3.1)$$

The complex amplitude $A(x, t)$ is common to all fields and obeys the GLE [4–6]

$$\tau_0 (\dot{A} + v_g A') = \mu (1 + ic_0) A + \xi_0^2 (1 + ic_1) A'' - \gamma (1 + ic_2) |A|^2 A \quad (3.2)$$

subject to the homogeneous BC,

$$A(x, t) = 0 \quad \text{at } x = 0, L. \quad (3.3)$$

Dot and primes denote temporal and spatial derivatives. This BC effectively imposes on the fields in GLE approximation the $N-T_{\text{cond}}$ condition: $T = T_{\text{cond}}$, $\delta u = 0$, and $w = 0$. The other BCs listed in Table 1 are not realizable within the GLE approximation since it enforces one common amplitude for all fields. However, we found that the NSE results for envelope profiles and growth lengths obtained with the $F-T_{\text{cond}}$ BC compare better with the GLE results. The GLE ansatz for the fields implies via the critical functions a spatially constant phase difference of $\frac{1}{2}\pi$ between δu and w . This is not the case for the NSE fields subject to the $N-T_{\text{cond}}$ BC, which show close to the boundaries a deviation from the above phase relation, while the $F-T_{\text{cond}}$ BC entails phase relations closer to those of the GLE.

All coefficients of the GLE, the critical numbers ϵ_c , k_c , ω_c , and the eigenfunction $\hat{u}(z)$ have been calculated [5] as functions of Re . As a consequence

of the system's invariance under the combined symmetry operation $\{x \rightarrow -x, Re \rightarrow -Re\}$ $\epsilon_c, k_c, \tau_0, \xi_0^2, \gamma$ are even in Re while ω_c , the group velocity v_g , and the imaginary parts c_0, c_1, c_2 are odd in Re [5,22]. For $\sigma = 1$ an expansion in Re yields $\epsilon_c \approx (Re/35.93)^2, k_c \approx 3.116[1 + (Re/99.97)^2], \omega_c \approx 3.6475Re, \tau_0 \approx 0.07693[1 - (Re/39.13)^2], \xi_0^2 \approx 0.148[1 - (Re/35.24)^2], v_g \approx 1.229Re, \gamma \approx 0.7027[1 - (Re/332.6)^2], c_0 \approx Re/140.1, c_1 \approx Re/39.98, c_2 \approx Re/387$ [5]. The next order terms are in each case two orders in Re higher.

3.2. Eigenvalue problem

Let us consider small through-flow rates Re and thermal stresses μ slightly above the boundary [13]

$$\mu_{\text{conv}}^c = \frac{\tau_0^2 v_g^2}{4\xi_0^2 (1 + c_1^2)} \quad (3.4)$$

between the absolutely and convectively unstable parameter regime. We solved the GLE (3.2) numerically with a Crank–Nicholson algorithm with a resolution of 20 grid points per unit length d [5,7]. The final state solution of (3.2) with the homogeneous BC (3.3) is of the form

$$A(x, t) = a(x)e^{-i\Omega t} = R(x)e^{i[\varphi(x) - \Omega t]}. \quad (3.5)$$

It oscillates harmonically with the global frequency

$$\Omega = \omega - \omega_c \quad (3.6)$$

under a stationary envelope $R(x)$ with a stationary wave number profile

$$q(x) = k(x) - k_c = \varphi'(x). \quad (3.7)$$

Inserting the solution ansatz (3.5) into the GLE one obtains the nonlinear eigenvalue problem

$$\begin{aligned} i\tau_0(-\Omega + v_g q)R + \tau_0 v_g R' \\ = \mu(1 + ic_0)R \\ + \xi_0^2(1 + ic_1)(R'' - q^2 R + iq'R + 2iqR') \\ - \gamma(1 + ic_2)R^3. \end{aligned} \quad (3.8)$$

The eigenvalue Ω and the associated eigenfunction $a(x) = R(x)e^{i\varphi(x)}$ describing dynamics and structure of the pattern are fixed by the BC (3.3). We

cannot make statements about the eigenvalue spectrum. But our numerical solutions of (3.2) suggest that initial conditions always evolve into a pattern with a smooth amplitude $a(x)$ with small frequency Ω . In that sense the eigenvalue problem (3.8) with the BC (3.3) resembles ground state problems of the Schrödinger equation – increasing the spatial variation of the wave function (amplitude a) implies higher kinetic energy (frequency Ω).

4. Pattern selection within the NSE for different boundary conditions

In this section we investigate how structure and dynamics of patterns selected in different through-flows are influenced by the lateral BC. We present numerical simulations of the full field equations in comparison with numerical solutions of the GLE. Results are often presented as functions of the scaled group velocity [4,7]:

$$V_g = \frac{\tau_0 v_g}{\xi_0 \sqrt{(1 + c_1^2)} \mu} = 2 \sqrt{\frac{\mu_{\text{conv}}^c}{\mu}} \quad (4.1)$$

which scales as $Re/\sqrt{\mu}$ for small Re (cf. Section 3). With this scaling the boundary between absolute and convective instability lies at $V_g = 2$ and thus allows direct comparisons for different μ – Re combinations. We have varied the Reynolds number at a fixed $\varepsilon = 0.215$. Thus we scan the Re – μ control parameter plane according to (2.10) along the path $\mu = 0.215/[1 + \varepsilon_c(Re)]$ that is slightly curved and that hits the borderline μ_{conv}^c (3.4) of the absolutely unstable regime at $Re \simeq 3.8$. Along this path V_g varies for $\sigma = 1$ as $V_g \approx 0.53Re + O(Re^3)$.

4.1. Selected frequency eigenvalues

In Fig. 1 we show NSE frequency eigenvalues (symbols) as functions of the scaled group velocity V_g (4.1) for the six BCs of Table 1 together with the GLE eigenvalue (full line) for N – T_{cond} conditions. Approaching the border to the convective instability at $V_g = 2$ the growth length of the patterns from the inlet increases

and the dependence of ω on the BC gets weak and all ω values come close together, whereas for small V_g much stronger differences can be observed. The selected frequencies are predominantly influenced by the inlet BC. A change of the outlet BC leads to ω -variations which are 10^{-3} – 10^{-5} times smaller than those induced by changing the inlet BC. This insensitivity of ω to the outlet BC reflects the different amplifying properties of perturbations in upstream or downstream direction. However, the intensity envelopes (Section 4.2) and the wave number profiles (Section 4.4) are more strongly influenced by the outlet BC, in particular in its vicinity.

From all BCs $N-T_{\text{cond}}$ leads to the largest and $F-Q_0$ to the smallest frequencies. In general a change in the inlet BC from N to F causes ω to decrease. For T_{cond} and T_0 conditions this change is small, whereas it becomes significant for the thermally insulating cases Q_0 . This can be explained by the different phase pinning properties of the different BCs. In the $N-T_{\text{cond}}$ case that enforces the basic state at inlet and outlet the temporal Fourier amplitudes of *all* convective fields drop to zero, leaving the phase indetermined and free to move. On the other hand, enforcing a von Neumann BC for one of the fields yields a nonvanishing field amplitude, a phase pinning effect, and therefore a reduction of the phase velocity. In the case of $F-Q_0$ the phase pinning is strongest, because there $\partial_x w$ as well as $\partial_x T$ vanish, leaving a free-phase condition only for u .

Both T_0 conditions induce a *large* stationary “boundary vortex” flow in the vicinity of the boundaries, that can be seen directly via the zeroth Fourier modes of the fields, e.g., δu_0 and indirectly via the lateral variation of, e.g., $|u_1|$ (cf. Section 4.2 and Fig. 2). It is quite similar to the stationary Ekman vortex structures that appear in the Taylor Couette system with through-flow as a result of a vanishing azimuthal velocity at inlet and outlet [7]. Besides that the lateral variation of $|u_1|$ induces for all BCs weaker stationary “flank vortices” (cf. Section 4.2 and Fig. 2) localized in the region of largest lateral growth of $|u_1|$. The stationary vortex structures exert an additional frictional force on the phase of the propagating vortices that reduces their phase velocity, when the fields δu_0 and u_1 spatially overlap. The frequency re-

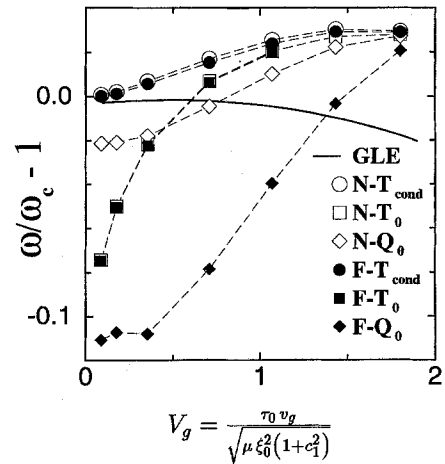


Fig. 1. Selected oscillation frequency of traveling convection rolls obtained from the NSE for different lateral BCs (symbols) and from the GLE for $N-T_{\text{cond}}$ BC (full line) versus the scaled group velocity V_g (4.1). Dashed lines are guides to the eye. Parameters are $\epsilon = 0.215$ and $\sigma = 1$.

duction roughly depends on the δu_0 -amplitudes of the stationary secondary vortex structures relative to the size of the propagating vortex amplitudes, say $|u_1|$. An analogous argument was given by Cross et al. [23] for the wave number selection at $Re = 0$. In this way one can understand (i) That the ω -reduction for T_{cond} and Q_0 boundaries saturates with decreasing V_g : For these BCs the magnitude of the δu_0 -amplitudes of the “flank vortices” approaches near the boundaries the size of $|u_1|$ from below when the $|u_1|$ -profile of the propagating structure comes closer and closer towards the inlet for $V_g \rightarrow 0$. (ii) That ω decreases for small V_g dramatically for T_0 -boundaries: They enforce stationary “boundary vortex” amplitudes $\delta u_0 > |u_1|$ such that $\delta u_0/|u_1|$ further increases when $V_g \rightarrow 0$. As an aside we mention that the decrease of $\omega/\omega_c - 1$ at small through-flow in the T_0 case differs from the otherwise very similar results for propagating vortex patterns in the rotating Couette system with Ekman vortex enforcing inlet/outlet conditions. There an increase of $k/k_c - 1$, i.e., of $\omega/\omega_c - 1$ has been observed for small Re [7, Fig. 6].

The GLE frequency eigenvalues (full curve in Fig. 1) deviate in a systematic manner from the NSE ones (open circles for the common $N-T_{\text{cond}}$ BC). This has also been found for downstream propagating

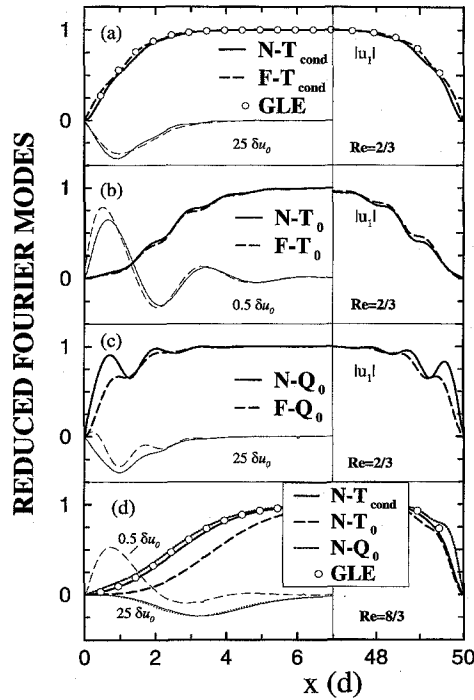


Fig. 2. Lateral profiles of convection structures for different BCs. Temporal Fourier modes $|u_1|$ and δu_0 reduced by the bulk value of $|u_1|$ at $x = 30$ are shown at $z = 0.225$ close to the inlet ($x = 0$) and outlet ($x = 50$) boundaries. For clarity δu_0 is suppressed in the outlet region $47 < x < 50$. Lines refer to NSE results and open circles to the GLE subject to $N-T_{\text{cond}}$ conditions. Parameters are $\epsilon = 0.215$ and $\sigma = 1$.

vortices in the Taylor Couette system [7]. The reason for this systematic deviation seems to be here as for propagating Taylor vortices the different dispersion relations of NSE and GLE. See Ref. [7] for a detailed discussion.

4.2. Lateral pattern profiles

In Fig. 2 we present the lateral variations of $|u_1|$ and δu_0 at $z = 0.225$ for two different Re values. The bulk region $7 < x < 45$ is cut out, because there the Fourier modes are almost constant. Since δu is zero at inlet and outlet for all our BCs this field allows best to elucidate the changes induced by different BCs. The lateral velocity δu has a further advantage for the analysis of the BC-dependence of convection patterns since δu is more sensitive to lateral BCs than, say, w : The lateral deformations in the flanks of the profiles of δu are more pronounced than for w . In our earlier work [4–6] where w profiles were analyzed we detected

only minor differences between NSE and GLE profiles where these deformations are completely absent.

The deformations in the lateral field profiles of, say $|u_1|$, are caused by the nonlinear couplings to a stationary vortex structure located in the flank regions where the lateral variation of the intensity $|u_1|$ of the propagating pattern is large. Typically the secondary flow amplitude δu_0 of the “flank vortices” reaches a strength of about 2% of the bulk $|u_1|$. The “flank vortex” flow increases when changing the BCs according to $N \rightarrow F$ and/or $T_{\text{cond}} \rightarrow T_0 \rightarrow Q_0$. The “flank vortices” associated with the inlet facing flanks of $|u_1|$ become weaker with increasing V_g since then the $|u_1|$ -profile becomes smoother as its growth length increases (see Fig. 2(d) for $Re = \frac{8}{3}$).

Besides this $|u_1|$ -induced stationary “flank vortex” flow, there is for the T_0 BC a boundary induced stationary “boundary vortex” structure of large amplitude $\delta u_0 \approx |u_1|$ which is very similar to the stationary Ekman vortex structure in the analogous Taylor

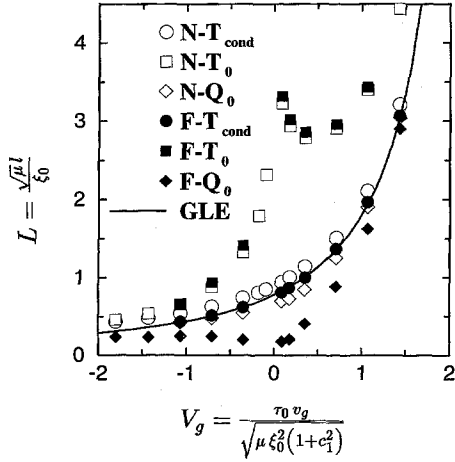


Fig. 3. Scaled growth lengths L of propagating convection patterns versus scaled group velocity V_g . Growth distances where $|u_1|$ reaches half its bulk value from inlet (outlet) are shown for positive (negative) V_g . Symbols refer to NSE results and line to GLE. Parameters are $\epsilon = 0.215$ and $\sigma = 1$.

Couette system [7]. This “boundary vortex” structure, induced by the T_0 BC, is always located near the lateral boundaries irrespective where the $|u_1|$ flanks are located and its intensity falls off towards the bulk – see δu_0 in Fig. 2(d) for $Re = \frac{8}{3}$.

For a more quantitative comparison of the selected amplitude’s profiles we have determined the characteristic growth lengths from inlet and outlet where $|u_1|$ reaches half of its bulk value. To that end we have performed a least-squares fit to $|u_1|$ with the function $(1 - c^{ax}) / (b + c^{ax})$ with fit parameters a and b in order to obtain also in the presence of amplitude deformations comparable results. This fit function yields good results except directly in the inlet region. In Fig. 3 we show the scaled growth lengths [4–6]

$$L = \sqrt{\mu} l / \xi_0 \tag{4.2}$$

of $|u_1|$ as a function of V_g . Note that inlet (outlet) growth lengths are shown for positive (negative) V_g . L has to be identical at inlet and outlet for $V_g = 0$. In addition L seems to have there a continuous first derivative for T_{cond} and Q_0 conditions but not for T_0 . For the latter BC L strongly increases as V_g approaches zero since the stationary “boundary vortex” induced by the T_0 condition strengthens with decreasing $|V_g|$ relative to $|u_1|$ and therefore pushes the oscillating pattern into

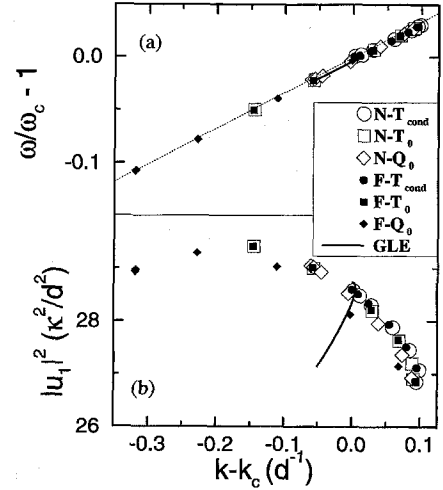


Fig. 4. (a) Frequency eigenvalues $\omega/\omega_c - 1$ and (b) bulk flow intensities $|u_1|^2$ versus selected bulk wave numbers $k - k_c$ of propagating roll patterns are shown for several Reynolds numbers covering the whole absolutely unstable regime $0 < V_g < 2$. Symbols (lines) refer to results obtained from the NSE with different BCs (GLE with $N-T_{\text{cond}}$ BC). The thin dotted curve in (a) shows $(k - k_c)v_g/\omega_c$ as discussed in Section 4.3. Parameters are $\epsilon = 0.215$ and $\sigma = 1$.

the bulk. Changing the BCs along the sequence $F-T_0 \rightarrow N-T_0 \rightarrow N-T_{\text{cond}} \rightarrow F-T_{\text{cond}} \rightarrow N-Q_0 \rightarrow F-Q_0$ decreases L successively. For both T_{cond} conditions GLE and NSE agree quite well with deviations being smaller for $F-T_{\text{cond}}$ BC than for $N-T_{\text{cond}}$ BC (see Section 3.1).

4.3. Phase relations in the bulk

Let us consider first the dispersion relation between the frequency ω , i.e., the temporal phase gradient and the spatial gradient k in the bulk part of the system. The GLE (3.8) predicts the relation

$$\tau_0 \Omega = (c_2 - c_0)\mu + \tau_0 v_g q_b + (c_1 - c_2)\xi_0^2 q_b^2 \tag{4.3}$$

between selected frequency $\Omega = \omega - \omega_c$, wave number $q_b = k_b - k_c$, and modulus $R_b^2 = (\mu - \xi_0^2 q_b^2) / \gamma$ for bulk patterns with $R'_b = R''_b = q'_b = 0$. Fig. 4(a) shows the GLE result (4.3) (full line) together with the NSE results (symbols) obtained for the six BCs for all Reynolds numbers sufficiently large to establish a bulk region with spatially constant wave number. Since the bulk GLE wave numbers are very close to the critical

one the quadratic contribution q_b^2 to Ω and to R_b is for all through-flow rates $0 < V_g < 2$ very small so that Ω is practically linear in k (Fig. 4(a)). That also holds for the NSE case. Here, however, the spread in the bulk wave numbers around k_c is considerably larger depending on the lateral BC and Re . Within the resolution of Fig. 4(a) the bulk dispersion relation for propagating roll vortices resulting from GLE or NSE reads

$$\omega \simeq \omega_c + v_g(k - k_c) \quad (4.4)$$

irrespective of the BC. The slight deviation between the thin dotted curve in Fig. 4(a) that represents $\omega/\omega_c - 1 \simeq (k - k_c)v_g/\omega_c$ according to (4.4) and the GLE result (full line) comes from the contribution $(c_2 - c_0)\mu/(\omega_c\tau_0)$ to the GLE dispersion relation (4.3).

In Fig. 4(b) we show the relation between bulk intensity $|u_1|^2$ of the propagating pattern and bulk wave number. Again the symbols (full line) denote the NSE (GLE) results for several Re and BCs. To determine $|u_1|^2$ for the GLE we have used (3.1) with the properly normalized linear eigenfunction $\hat{u}(z)$ [24] evaluated at $Re = 0$. The relations between bulk pattern amplitude and bulk wave number resulting from NSE and GLE are obviously quite different. The peculiar shape of the full curve in Fig. 4(b) which seems to be at first sight at odds with the GLE formula $R_b^2 = \mu - \xi_0^2 q_b^2$ is caused by two facts: (i) Due to the pattern selection process the selected wave number in the bulk region is uniquely determined by the control parameters μ , Re . For a given μ one obtains for $Re = 0$ the critical wave number [23]. Then, with increasing Re the wave number first slightly increases and later on it decreases below the critical one to the value

$$\xi_0 q_b = -\frac{\sqrt{1 + c_1^2} - \sqrt{1 + c_2^2}}{c_1 - c_2} \sqrt{\mu_{\text{conv}}^c} \quad (4.5)$$

at the border between absolute and convective instability [7]. (ii) The contribution from $\xi_0^2 q_b^2$ to R_b^2 is very small since $|q_b| \lesssim 0.05$. Therefore the variation of R_b^2 and thus of $|u_1|^2$ is mainly caused by monotonously decreasing $\mu = 0.215/[1 + (Re/35.93)^2]$ while increasing Re from $Re = 0$ to $Re \simeq 3.8$ where $V_g = 2$.

4.4. Wave number profiles

Having investigated the frequency eigenvalue and the modulus profile $|u_1|$ of the associated eigenfunction we now address its phase structure. The frequency eigenvalue and the lateral profile of the phase gradient $k(x) = \partial_x \varphi_1(x)$ seem to be closely tied together. The latter is largely slaved by the envelope profile $|u_1|$ which itself is most strongly influenced by the BCs.

Figure 5 shows selected modulus profiles of $|u_1|$ together with corresponding wave number profiles $k(x)$ for a small through-flow with $Re = \frac{1}{6}$. The inlet boundary conditions were $N-T_{\text{cond}}$ or $F-Q_0$ and the outlet conditions were always $N-T_{\text{cond}}$. The frequencies for these two inlet BCs differ significantly (cf. Fig. 1) and also the wave number profiles $k(x)$ are quite different. Large deformations in the pattern amplitude $|u_1|$ cause strong deformations of the phase gradient $k(x)$. So both, the temporal derivative ω and the spatial gradient $k(x)$ of the phase of the propagating pattern, are influenced by the inlet BC. Note also that the (boundary induced) deformations of the pattern profile $|u_1|$ correlate with corresponding variations of $k(x)$. The GLE, on the other hand, yields a wave number profile (open circles in Fig. 5(b)) that is very close to k_c and that is practically constant (cf. [7, Fig. 4(b)] for more details) in space while the NSE wave numbers show significantly larger variations.

In the inset of Fig. 5 we show $k(x)$ in the bulk region $10 < x < 45$ where $|u_1|$ is almost constant. For the phase pinning $F-Q_0$ BC the wave number does not saturate into a bulk part for the small through-flow of $Re = \frac{1}{6}$. Instead $k(x)$ shows an exponential growth (full line in the inset of Fig. 5) in the region of bulk pattern amplitude from small k in the upstream portion to large k in the downstream region: For sufficiently small through-flow the phase pinning forces at the inlet are strong enough to cause an elongation of the pattern, i.e., a decrease in k near the inlet that heals out exponentially in downstream direction. Increasing Re or decreasing the inlet phase pinning with other BCs reduces the pattern elongation, i.e., the wave number gradients. On the other hand, decreasing Re increases the gradient of $k(x)$ and eventually even suppresses the phase propagation altogether. This latter transition

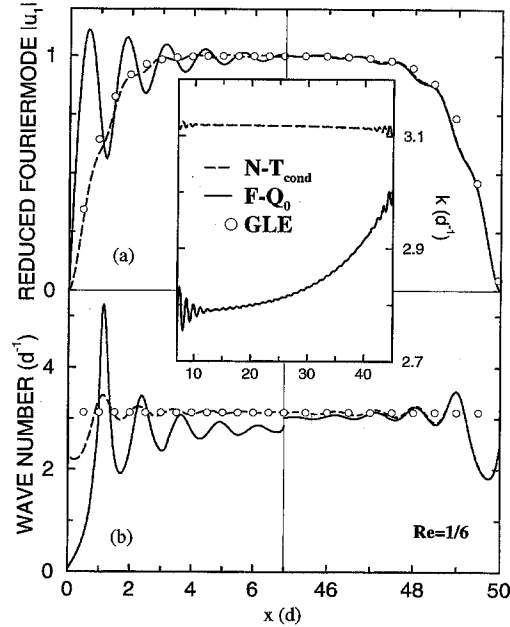


Fig. 5. (a) Amplitude profiles and (b) wave number profiles close to inlet and outlet. The temporal Fourier mode $|u_1|$ of the traveling convection pattern was reduced by the bulk value at $x = 30$. The inset shows the lateral variation of the wave number in the center region of the system. The outlet BC was $N-T_{\text{cond}}$, the inlet BCs are indicated in the inset. Parameters are $\epsilon = 0.215$ and $\sigma = 1$.

at very small Re depends on the system size – cf. Ref. [5] for a related detailed investigation.

However, when the parameters are such that a true bulk part of the pattern is established in which amplitude and wave number are constant then the selected frequency and lateral pattern profile seem to be independent of the system size. This always occurs in sufficiently large systems when the through-flow is sufficiently strong.

5. Conclusion

We have investigated convection roll structures in systems of finite length that propagate downstream in an externally applied lateral flow with roll axes perpendicular to the flow direction subject to six different inlet/outlet BCs. Within the absolutely unstable parameter regime a unique pattern selection is observed. The selected convection patterns are independent of parameter history, initial condition, and system length provided the latter is large enough to allow for a sat-

urated bulk region with homogeneous pattern amplitude and wave number. But they depend on the lateral BC. The outlet BC influences the convection structures only locally in the vicinity of the outlet while the globally constant frequency and the lateral profiles of pattern amplitude and wave number and their bulk values are basically determined by the inlet BC. The selected frequency ω of the pattern oscillation is an eigenvalue of a nonlinear eigenvalue problem with the set of time periodic convection fields, $f(x, z, t) = f(x, z, t + 2\pi/\omega)$, being the associated eigenfunction. The analysis of the appropriate GLE approximation suggests that the eigenfunction associated to the selected eigenfrequency varies as smoothly and as little as possible under the imposed BC. This property is similar to the ground state behavior of the linear stationary quantum mechanical Schrödinger equation.

Different lateral BCs entail different frequencies and eigenfunctions, i.e., lateral pattern profiles. For example, inlet conditions that exert a phase pinning force on one or more of the fields of traveling convection rolls reduce the frequency. The spatial growth

behavior and the pattern profile of the convective structures in the region between inlet and bulk saturated pattern is strongly influenced by the inlet BC and can be quite intricate. While the frequencies and bulk wave numbers obtained for various BCs and through-flow rates well inside the absolutely unstable regime differ substantially they all fall onto a linear dispersion curve. Finally, when approaching with increasing Re the border between absolute and convective instability the eigenfrequencies and also the spatial pattern profiles belonging to different BCs approach each other – with increasing growth length of the pattern from the inlet the influence of the latter on spatiotemporal properties of the convection pattern becomes weaker.

Acknowledgements

This work was supported by the Stiftung Volkswagenwerk.

References

- [1] M.C. Cross and P.C. Hohenberg, *Rev. Mod. Phys.* 65 (1993) 851.
- [2] F.H. Busse, *Rep. Prog. Phys.* 41 (1978) 1929.
- [3] R.C. DiPrima and H.L. Swinney, in: *Hydrodynamic Instabilities and Transition to Turbulence*, eds. by H.L. Swinney and J.P. Gollub (Springer, Berlin, 1981) p. 139.
- [4] H.W. Müller, M.Lücke and M. Kamps, *Europhys. Lett.* 10 (1989) 451.
- [5] H.W. Müller, M. Lücke and M. Kamps, *Phys. Rev. A* 45 (1992) 3714.
- [6] H.W. Müller, M. Lücke and M. Kamps, in: *Ordered and Turbulent Patterns in Taylor Couette Flow*, eds. by D. Andereck and F. Hayot, NATO ASI Series B Vol. 297 (Plenum, New York, 1992), p.187.
- [7] P. Büchel, M. Lücke, D. Roth and R. Schmitz *Phys. Rev. E* 53 (1996) 4764.
- [8] A. Bers, in: *Basic Plasma Physics I*, eds. A.A. Galeev and R.N. Sudan (North-Holland, New York, 1983); R.J. Briggs, *Electron Stream Interaction with Plasmas* (MIT Press, Cambridge, MA, 1964).
- [9] H.A. Snyder, *Proc. Roy. Soc. London Ser. A* 265 (1961) 198; *Ann. Phys.* 31 (1965) 292; K.W. Schwarz, B.E. Springett and R.J. Donnelly, *J. Fluid Mech.* 20 (1964) 281; R.J. Donnelly and D. Fultz, *Proc. Nat. Acad. Sci. USA* 46 (1960) 1150; D.J. Takeuchi and D.F. Jankowski, *J. Fluid Mech.* 102 (1981) 101; Z.H. Gu and T.Z. Fahidy, *Can. J. Chem. Engrg.* 63 (1985) 710; 63 (1985) 14; 64 (1986) 185; R.M. Lueptow, A. Docter and K. Min, *Phys. Fluids A* 4 (1992) 2446; N. Gravas and B.W. Martin, *J. Fluid Mech.* 86 (1978) 385; P.L. Greaves, R.I. Grosvenor and B.W. Martin, *Int. J. Heat and Fluid Flow* 4 (1983) 187; D.A. Simmers and J.E.R. Coney, *J. Mech. Engrg. Sci.* 21 (1979) 59; M.M. Sorour and J.E.R. Coney, *J. Mech. Engrg. Sci.* 21 (1979) 397. K. Kataoka, H. Doi, T. Hongo and M. Futagawa, *Chem. Engrg. of Japan* 8 (1975) 472; K. Bühler and F. Polifke, in: *Nonlinear Evolution of Spatio-temporal Structures in Dissipative Continuous Systems*, eds. by F. Busse and L. Kramer (Plenum Press, New York, 1990) p. 21.
- [10] J.K. Platten and J.C. Legros, *Convection in Liquids* (Springer, Berlin, 1984).
- [11] K.L. Babcock, G. Ahlers and D.S. Cannell, *Phys. Rev. Lett.* 24 (1991) 3388; *Phys. Rev. E* 50 (1994) 3670; K.L. Babcock, D.S. Cannell and G. Ahlers, *Physica D* 61 (1992) 40.
- [12] A. Tsameret and V. Steinberg, *Europhys. Lett.* 14 (1991) 331; *Phys. Rev. E* 49 (1994) 1291; 67 (1991) 3392; A. Tsameret, G. Goldner and V. Steinberg, *Phys. Rev. E* 49 (1994) 1309.
- [13] R.J. Deissler, *J. Statist. Phys.* 40 (1985) 371; 54 (1989) 1459; *Physica D* 25 (1987) 233; 18 (1986) 467.
- [14] L.D. Landau and E.M. Lifshitz, *Fluid Mech.* (Pergamon Press, Oxford, 1959).
- [15] G.Z. Gershuni and E.M. Zhukhovitskii, *Convective Stability of Incompressible Fluids* (Keter Press, Jerusalem, 1976).
- [16] S. Chandrasekhar, *Hydrodynamic and Hydromagnetic Stability* (Dover, New York, 1981).
- [17] K.S. Gage and W.H. Reid, *J. Fluid Mech.* 33 (1968) 21.
- [18] S.H. Davis, *J. Fluid Mech.* 30 (1967) 465.
- [19] K. Stork and U. Müller, *J. Fluid Mech.* 54 (1972) 599.
- [20] J.M. Luijckx, J.K. Platten and J.C. Legros, *Int. J. Heat Mass Transfer* 24 (1981) 1287.
- [21] J.M. Luijckx, Ph.D. Thesis, University of Mons, Belgium (1983).
- [22] A. Recktenwald, M. Lücke and H.W. Müller, *Phys. Rev. E* 48 (1993) 4444.
- [23] M.C. Cross, P.G. Daniels, P.C. Hohenberg and E.D. Siggia, *J. Fluid Mech.* 127 (1983) 155.
- [24] C. Jung, private communication.